Journal of Power Sources 271 (2014) 538–547

Contents lists available at ScienceDirect

Journal of Power Sources

journal homepage: www.elsevier.com/locate/jpowsour

The effect of pre-oxidation treatments on the oxidation tolerance of Ni-yttria-stabilized zirconia anodes in solid oxide fuel cells

J.L. Young, H. Molero, V.I. Birss*

Department of Chemistry, University of Calgary, Calgary, Alberta T2N 1N4, Canada

HIGHLIGHTS

- SEM/XPS demonstrate NiO ejection onto Ni-YSZ anode surface after redox cycling.
- NiO ejection reflects stress reduction of anode as Ni to NiO expansion occurs.
- Anodes were pre-oxidized to 75% NiO at 600 °C to pre-eject NiO (no cracks form).
- Pre-oxidation improves subsequent redox tolerance at 600 °C.
- Pre-oxidation decreases crack severity by 50% during air exposure at 800 °C.

ARTICLE INFO

Article history:
Received 2 April 2014
Received in revised form
11 July 2014
Accepted 27 July 2014
Available online 19 August 2014

Keywords:
Ni-YSZ
Nickel oxidation
Redox cycling
Solid oxide fuel cells (SOFC)
Electrolyte cracking

ABSTRACT

When a Ni-YSZ (yttria-stabilized zirconia) anode-supported solid oxide fuel cell (SOFC) is exposed to air at high temperatures, the outcome can be catastrophic cell degradation (primarily YSZ electrolyte cracking), resulting from the 70% volume expansion of Ni as it forms NiO. Earlier work showed that the damage is less severe under conditions when no gradient in the NiO content into the Ni-YSZ support layer was allowed to develop during the oxidation process (e.g., oxidation at 600 °C). This was correlated with qualitative scanning electron microscopy observations, showing that NiO particles are ejected out of the Ni-YSZ/air surface. In the present work, XPS analysis confirmed the enrichment of NiO at the outer anode surface, suggesting that it may be possible to pre-oxidize the Ni-YSZ support layer at 600 °C to force some NiO out onto the anode surface and thus enhance cell oxidation tolerance. It is shown here that, following pre-oxidation at 600 °C, the amount of Ni oxidation tolerated prior to electrolyte cracking at 600 °C increased from 75% to 80%. For oxidation at 800 °C, following pre-oxidation at 600 °C, electrolyte cracking was less severe, but cracks still appeared before 50% of the Ni in the anode was oxidized.

1. Introduction

Solid oxide fuel cells (SOFCs), which can convert the chemical energy of a fuel (H_2, H_2 + CO, CH_4, etc.) to electricity and heat with very high efficiency, typically utilize a nickel-yttria stabilized zirconia (Ni-YSZ) cermet as the anode material. Ni-YSZ anodes have very good chemical and physical stability in reducing environments, a high electrocatalytic activity for hydrogen oxidation [1], and good manufacturability. Cells that utilize Ni-YSZ anodes as the support layer are advantageous because the Ni-based cermet provides the mechanical support of the cell and has a low resistance. This architecture allows the cathode and the YSZ electrolyte, which have a higher resistivity, to be made very thin, lowering the operating temperatures to <750 °C from 1000 °C [1–3].

One of the challenges facing Ni-based anode-supported cells is that, if they are inadvertently exposed to air (e.g., if air enters the anode chamber during an emergency shutdown) while at operating temperatures of >600 °C, the Ni component can rapidly oxidize (Reaction (1)) [4]. The large volume expansion (>65%) associated with the conversion of Ni to NiO causes significant cracking of the thin (~10 μm) electrolyte in a relatively short period of time (due to the rapid oxidation kinetics of Ni) [4–7]. The more severe the cracks, the greater the cell performance losses are, due primarily to fuel and air leakage. This damage occurs despite the fact that the anodes are fabricated in an oxidized state. This is due to sintering mechanisms that alter the Ni morphology after it is reduced at high temperatures [8].

$$Ni + 1/2\ O_2 \rightarrow NiO \quad (1)$$

Currently, system solutions that are commonly utilized to prevent cell damage arising from oxidation of the Ni anode include the

* Corresponding author. Tel.: +1 403 220 6432; fax: +1 403 289 9488.
E-mail address: birss@ucalgary.ca (V.I. Birss).

http://dx.doi.org/10.1016/j.jpowsour.2014.07.174
0378-7753/

use of a valve that functions in the hot zone [9] or purging the anode with N_2 during start-up and shut-down [10]. However, cost and practicality (especially in remote or distributed generation applications) make some of these solutions impractical. Thus, it is desirable for SOFCs to have some degree of 'oxidation tolerance', which refers to the ability of the Ni in the anode to be exposed to oxygen or air at high temperatures with little or no performance degradation observed. Various approaches for improving the oxidation tolerance of Ni-YSZ anodes have been examined, such as the use of ceramic dispersions (e.g., CaO, MgO and TiO_2) in the Ni phase to prevent agglomeration [11], or the grading of the Ni content in the screen printed anode layers adjacent to the electrolyte, which has a decreased porosity as compared to the support layer [12]. However, cell modifications have not been implemented due to limitations in manufacturability, high materials and manufacturing costs, or due to a resulting significant loss in cell performance.

There has been significant work done [13–21], aimed at establishing the limits of exposure of Ni-YSZ anode-supported cells to air, showing that, if the strain on the cell exceeds 0.1% [13,14], then the electrolyte will crack. In addition, it has been shown [13] that a higher porosity in the anode layer increases the tolerance of the cell to Ni oxidation. Further, electrolyte cracking during Ni oxidation is more severe (based on the width and the number of cracks in the YSZ electrolyte) as the isothermal oxidation temperature is increased from 600 to 900 °C [6,15]. However, it was also shown [22], using a range of pO_2 atmospheres, that the extent of electrolyte cracking correlates with the gradient in the NiO content through the anode thickness over the course of air exposure, rather than being related to thermal shock.

There was some evidence for the build-up of NiO at the Ni-YSZ anode/air interface [22] under oxygen exposure conditions that minimized the transient NiO gradient through the anode layer. This suggested that the expulsion of NiO particles at the outer anode surface relieves the internal stresses in the anode and minimizes YSZ electrolyte cracking. It has been demonstrated [8] *in situ* in an environmental SEM that, during the high temperature oxidation of a Ni-YSZ anode, NiO particles will push into voids within the anode layer and out of the ASL surface. It was proposed [5,7] that the ejection of NiO particles (after reduction to Ni) leads to improved electrical contact to the current collectors and may also explain the increase in the conductivity of the ASL after Ni oxidation. This ejection of some of the NiO particles out of the anode-air interfacial region towards the outer surface could be a mechanism by which the stress on the YSZ electrolyte during the oxidation of the Ni phase within a Ni-YSZ ASL is lowered.

A series of schematic diagrams, shown in Figs. 1A–I, depicts the ejection of NiO particles during Ni-YSZ anode layer oxidation. Fig. 1A shows the Ni-YSZ anode in its initially reduced state and also gives a legend explaining the color scheme (in the web version) used for each particle in all of the diagrams in Fig. 1. All of the particles shown are drawn roughly to scale, based on the extent of oxidation of each particle, where the radius of the particles is assumed to increase from 1 μm (pure Ni) to 1.2 μm (fully converted to NiO), resulting in a 70% volume increase. The YSZ particles are shown to have a constant radius of 1.1 μm in each of these schematic drawings (Fig. 1).

The case when the oxidation conditions have resulted in a uniform Ni/NiO distribution throughout the anode support layer is shown in Fig. 1B–E (left side), while the case when the oxidation conditions have produced a gradient in the NiO distribution into the depth of the anode layer is shown in Fig. 1F–I (right side). The fraction of Ni in the anode layer that has been oxidized (oxidation depth) is portrayed in each diagram (Fig. 1) by the ratio of the NiO (green (in the web version)) to Ni (gray) areas. Thus, Fig. 1B

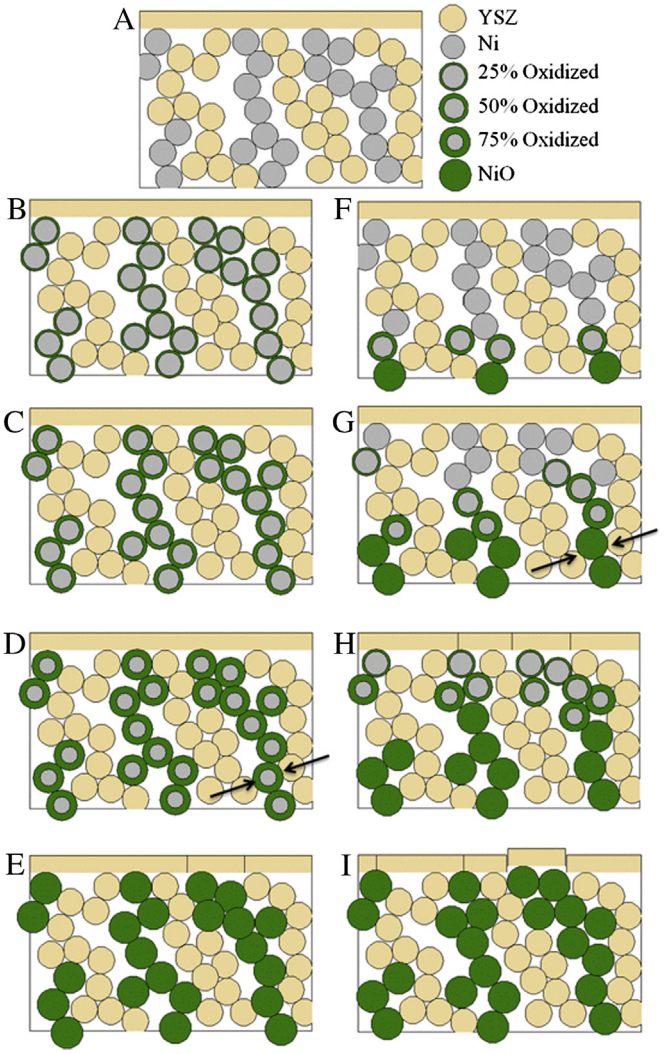

Fig. 1. Schematic showing (A) a single Ni-YSZ anode microstructure in which the anode layer is oxidized, either homogeneously (B, C, D, E) or with a gradient into the ASL (F, G, H, I), to an extent of (B,F) 25%, (C,G) 50%, (D,H) 75% and (E,I) 100% of the full Ni content. Under homogeneously oxidation conditions (B–E), as individual Ni particles reach 75% oxidation (D), they push against the YSZ particles (indicated by arrows), become pinned, and prevent further ejection of NiO to the outer surface. In the graded case (F–I), this pinning occurs at a lower % Ni oxidation (G) and thus fewer NiO particles are pushed out of the anode/air interface (shown at the base of each diagram).

(depicted the case of homogeneous oxidation into depth of anode layer) and 4F (graded oxidation conditions) both represent an anode layer in which 25% of the total Ni content is oxidized. The oxidation depth for both the homogeneous (Fig. 1B–E) and graded (Fig. 1F–I) cases is seen to increase by 25% in each diagram until the anode layer is fully oxidized (Fig. 1E and I).

It can be seen that, as the oxidation depth of the anode in the homogeneous oxidation case progresses from 25% in Fig. 1B to 75% in Fig. 1D, the interconnected Ni/NiO particles on the right side of the diagram, for example, are not wedged against the particles in the YSZ skeleton until ~75% of the total Ni content is oxidized, as indicated by the arrows in Fig. 1D. By this time, local stresses within the anode layer will have already served to eject a substantial amount of NiO out of the anode surface plane at the base of Fig. 1E.

However, in the graded NiO content case (Fig. 1F–I), the outer air-exposed edges and the face of the anode will be preferentially oxidized first and then these Ni/NiO particles (designated by the arrows in Fig. 1G) could wedge themselves against the YSZ skeleton

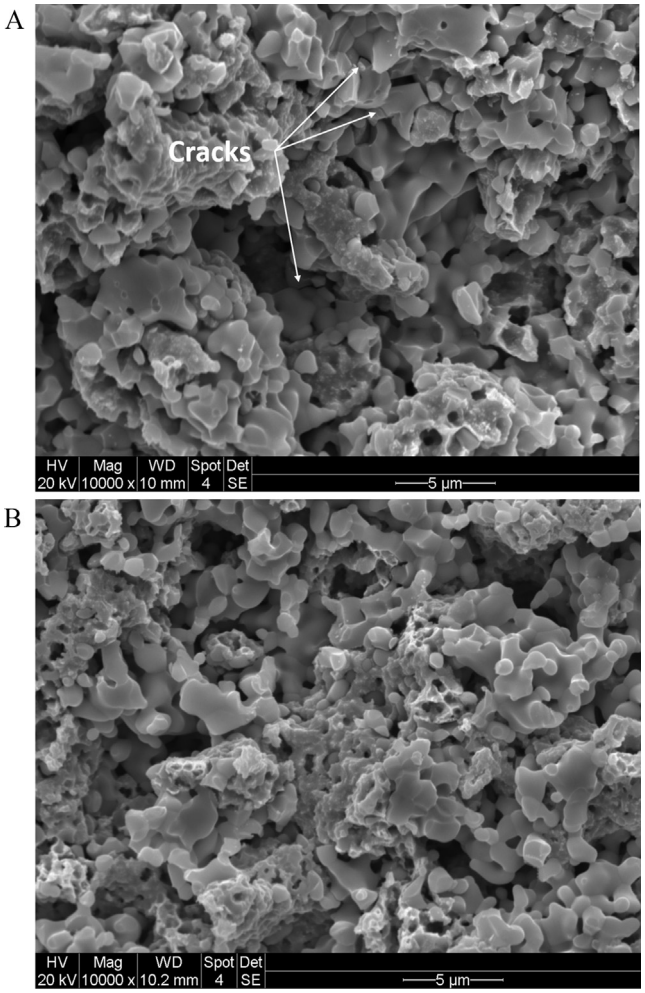

Fig. 2. SEM images of the cross-section of Ni-YSZ support layer after full oxidation of the Ni component at (A) 800 and (B) 600 °C. In each case, the sample has been fractured to expose the cross-section. It can be seen that cracks in the YSZ backbone are visible in the sample oxidized at 800 °C (A), while no cracks in the YSZ backbone are visible in the sample oxidized at 600 °C (B).

in the Ni-YSZ anode when between 25% (Fig. 1F) and 50% (Fig. 1G) of the total Ni content has been oxidized. Thus, after only 50% of the Ni is oxidized, no more NiO would be ejected out onto the outer anode surface. As Ni oxidation proceeds further, less NiO would be expelled from the Ni-YSZ anode at the anode/air interface (Fig. 1I) and, as a result, more NiO would remain inside the anode structure, which will increase the tensile stress exerted on the thin YSZ electrolyte.

The aim of the present study, therefore, was to confirm that enrichment of the NiO content at the anode/air interface develops under these homogeneous Ni oxidation conditions and to test the model shown in Fig. 1. This knowledge was then taken used to apply a "pre-oxidation" step to the cell in order to make the cell more oxidation tolerant. It was assumed that pre-oxidizing an anode to a safe level of oxidation prior to normal cell operation would result in the expulsion of some NiO out of the anode pore structure. After re-reduction, this Ni would remain on the outer surface of the anode layers and would not be involved in the degradation of a cell during any future oxidation cycles. Thus, the oxidation tolerance of the cell should be increased without modifying the manufacturing procedure of the cells. It is confirmed here that NiO is indeed enriched at the ASL (anode support layer)/air interface under conditions that result in less damage of cells due to Ni oxidation. It is also shown that, while the severity of electrolyte cracking due to oxidation at 800 °C can be decreased by the application of a pre-oxidation step, cell damage due to air exposure at high temperatures cannot be fully prevented.

2. Experimental methods

2.1. Sample details

The 17 mm diameter samples (post-sintering) used for the purpose of this study consisted of a Ni-YSZ anode support layer (ASL, 1 mm thick), a Ni-YSZ anode functional layer (AFL, 20 μm thick) and a thin, dense YSZ electrolyte layer (10 μm). The electrolyte side of the samples was not coated with a cathode or a counter electrode layer, and thus these samples were not operated electrochemically. This geometry was useful for mass measurements, as there was no cathode material present that could contribute to the observed mass change. Another advantage was that this design facilitated imaging analysis of either the electrolyte surface, to determine the extent of its cracking after exposure of the samples to a range of air exposure conditions, or the ASL surface, to seek the enrichment of the NiO particles.

The samples were prepared by first tape casting a 1 mm thick Ni-YSZ ASL (using 1 μm diameter NiO and YSZ particles) and then screen printing two layers of Ni-YSZ paste onto the tape cast ASL in order to form the AFL (functionalized by the use of finer 0.5 μm diameter NiO and YSZ particles) [23]. After this, two layers of a dense YSZ electrolyte layer (10 μm final thickness) were sequentially screen-printed onto the AFL, followed by drying at 80 °C after the deposition of each screen printed layer, and then co-firing at 1450 °C for 2 h. Both the ASL and AFL contained 57% (by mass) NiO and 43% YSZ, although the ASL was fabricated with a 1 μm average NiO and YSZ particle size versus a 0.5 μm starting particle size for the AFL. Prior to NiO reduction, the ASL and AFL had a porosity of 22% and 14%, respectively, while after NiO reduction, the ASL porosity increased to 39% and the AFL porosity to 30% (measured using AnalySIS® software).

2.2. Instrumentation

2.2.1. Thermogravimetric analysis (TGA)

All partial and full oxidation cycles were carried out inside a Setaram TAG 16 TGA/DSC symmetrical balance to allow tracking of the sample mass under various conditions, thus determining the extent of Ni oxidation/NiO reduction within the Ni-YSZ anode layers. Samples (200–250 mg fragments, formed by sectioning pieces from the full disc specimen) were placed (electrolyte down) in a shallow 100 μL Pt crucible. The Setaram TGA requires a backing gas and thus all gas concentrations involved a >50% He flow. Air was simulated with 20% O_2–He and reducing conditions were achieved with a gas flow of 10% H_2–He, with all exposures to H_2 and O_2 interspersed with a 15 min purge with 20% N_2–He to avoid mixing H_2 and O_2 inside the TGA instrument.

All of the samples were first heated to 600 or 800 °C in 20% N_2–He at 5 °C min^{-1} and then held there for 15 min to allow the temperature to stabilize. The H_2 (10% H_2 in He) flow was switched on for up to 12 h to ensure full (>99%) reduction of NiO. Samples were then exposed to 20% O_2–He (after a 10 min N_2 purge) for various time periods to achieve the controlled partial oxidation of the Ni component of the AFL and ASL. The samples were then immediately exposed to 20% N_2–He and cooled to room temperature at 7.5 °C min^{-1}. After microscopic characterization, the cell was then re-inserted into the TGA and heated to 600 or 800 °C, re-reduced, and then subjected to the next oxidation cycle.

The measured mass change of an anode for full oxidation or reduction was typically within ±0.2% of the theoretical value (based on the addition of 57 wt% NiO) [22], although at low temperatures (600 °C), the mass loss in the first reduction cycle could be as much as 0.5% below the theoretical mass change expected. This 0.5% mass difference is due to NiO that is trapped deep inside a layer of Ni, which substantially hinders NiO reduction. Subsequent oxidation and reduction cycles at 600 °C will liberate this NiO in the particle core [22], resulting in a mass change during these subsequent cycles that approaches ±0.2% of the theoretical value.

Errors in the mass measurements could also theoretically arise from the presence of more than one Ni oxidation state in the Ni oxide. Prior studies [24] have shown that the transition from Ni(II) oxide to Ni proceeds directly without any intermediate phases, but the Ni(III) content of fully oxidized Ni should range from 0.08 atom % at 870 °C to 0.5 atom% at 540 °C [25]. While the total mass gain or loss in our prior work [22] and in the present study never exceeded 100% of the theoretical value, this does introduce a small error as the Ni oxidation temperature is decreased. Thus, due to the high precision of our TGA instrument (±2 μg) and to the low Ni(III) content, the mass measurements can be considered to be very accurate.

2.2.2. SEM analysis

Sample imaging was carried out using a Philips FEI XL-30 Environmental Scanning Electron Microscope (SEM, 20 kV, 10 mm working distance) in vacuum mode to examine (Au-coated) surfaces of either the electrolyte or the Ni-YSZ ASL surface. The cell was attached perpendicularly to an Al stub covered with double-sided carbon tape, so that the cell cross-section was facing upwards to facilitate viewing.

2.2.3. XPS analysis

A Physical Electronics PHI VersaProbe 5000-XPS (X-ray photoelectron spectroscopy) instrument was used to record the XPS spectra. The spectra were collected using a monochromatic Al source (1486.6 eV) with a beam diameter of 200.0 μm. The binding energies were reported relative to the C1s peak at 285 eV. All samples were mounted after full oxidation without further treatment and pumped down from atmospheric pressure to ultrahigh vacuum (10^{-10} Torr). A wide energy survey was carried out (0–1400 eV) using a 187 eV pass energy to identify and quantify all the elements in the sample. A narrow energy spectrum (10–30 eV) was then acquired with a pass energy of 23 eV (for improved energy resolution) to determine the chemical state of the elements in the sample. The area of the most intense peak for each element was divided by the element-specific sensitivity factor and normalized to 100% to obtain the relative at% of each of the elements present in the sample.

3. Results and discussion

3.1. Evidence to support the mechanism of stress relief by NiO ejection out of the anode–air interface

High porosity (39%) Ni-YSZ anode support layers, covered with a thin Ni-YSZ AFL (30% porous) and then a thin YSZ electrolyte (20–30 mm^2 in area, no cathode layer attached), were studied extensively in prior studies [6,22]. It was noted [22] that, the more extreme the difference in NiO content between the outer and inner regions of the anode layer (achieved at high temperatures (>700 °C) or in low pO_2 (0.1% O_2) environments) over the course of air exposure of the anode, the higher the degree of degradation. Under these conditions, cracks in the thin electrolyte were seen when the percentage of total Ni in the anode layer that had been oxidized (defined as 'oxidation depth') was 40% [22]. Conversely, under conditions that lead to homogeneous Ni oxidation, it was shown that the electrolyte will not crack until an oxidation depth of ≥74% is reached [22].

A mechanism to explain this difference in oxidation tolerance has been expounded in Fig. 1. In this mechanism, it is postulated that the outer regions of the anode oxidize first and pin the NiO against the YSZ backbone in the anode layers and, as Ni oxidation progresses, the stress on the electrolyte is much higher than in the case when Ni oxidation is homogeneous throughout the anode layer. However, less cracking of the thin YSZ electrolyte when Ni oxidation throughout the Ni-YSZ anode thickness is uniform only indicates that the tensile stresses on the electrolyte are lower when the oxidation temperature is lowered.

The mechanism of stress relief by NiO ejection during oxidation should be evident by the amount of NiO ejected at the surface and by any sign of NiO pressing on the YSZ backbone. However, the detection of NiO pressing on the YSZ backbone of an anode support layer would be very difficult due to the inherent microstructural variability within the anode. Even so, it can be seen in Fig. 2 that there are cracks in the YSZ backbone throughout the anode layer in the sample that was fully oxidized at 800 °C. These cracks do not propagate through the full thickness of the anode layer, as seen in Fig. 2, but simply fracture the YSZ backbone locally. These cracks are not seen in the sample oxidized at 600 °C (Fig. 2B), suggesting that Ni oxidation at higher temperatures is indeed causing greater stress on the YSZ backbone.

However, another reason for the difference in internal stresses within the anode layer could result when Ni is oxidized at different temperatures is a change in NiO morphology resulting from Ni oxidation at different temperatures. An altered morphology would result in similar cracks in the YSZ electrolyte and in the anode layer. To compare the NiO morphology, SEM images of samples oxidized at 600 and 800 °C are shown in Fig. 3A and B, respectively, showing the air-side of a Ni-YSZ ASL after 100% oxidation of the Ni component in a single oxidation cycle.

It can be seen that, in both cases (Fig. 3A and B), a cellular structure results. However, it is also seen that the NiO formed at 600 °C (Fig. 3A) has a smaller average particle size (~0.4 μm) than that formed at 800 °C (~0.6 μm). Further, the NiO formed at a higher temperature has a morphology that indicates that it may actually be somewhat less porous. This observed porosity trend would result in higher internal stresses at low Ni oxidation temperatures, the opposite of what is actually seen [22]. Thus, it is likely that a change in NiO morphology is not responsible for the increase in electrolyte cracking that is observed [22] as the oxidation temperature is increased.

3.2. Confirmation of Ni ejection at anode/air interface using XPS

In Fig. 3, more NiO is seen on the surface after oxidation of a Ni-YSZ layer at 600 °C than at 800 °C. However, the natural variability of the morphology of these anodes is very high and the changes in the amount of NiO that are present on the outer surface are subtle. As it is difficult to conclusively determine if there is a reliable trend in the SEM micrographs, other techniques must be used to demonstrate these differences more clearly.

To verify the enrichment of NiO at the anode layer/air interface after air exposure at different temperatures, X-ray photoelectron spectroscopy (XPS) of the outer anode surface was employed. XPS has the advantage that it can be used to determine the NiO surface content over a large area, which minimizes the inherent surface morphology variability that results from the fabrication process used. The shallow penetration depth of analysis is also an

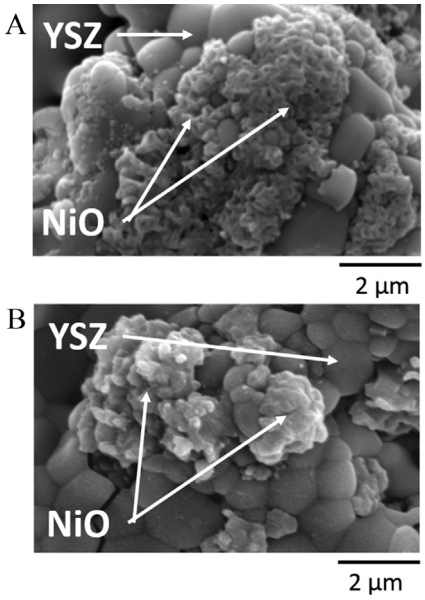

Fig. 3. SEM images of the air-side of a Ni-YSZ support layer after full oxidation of Ni component at (A) 600 and (B) 800 °C. NiO is distinguishable from YSZ by its finer grained structure and apparent roughness in comparison with YSZ.

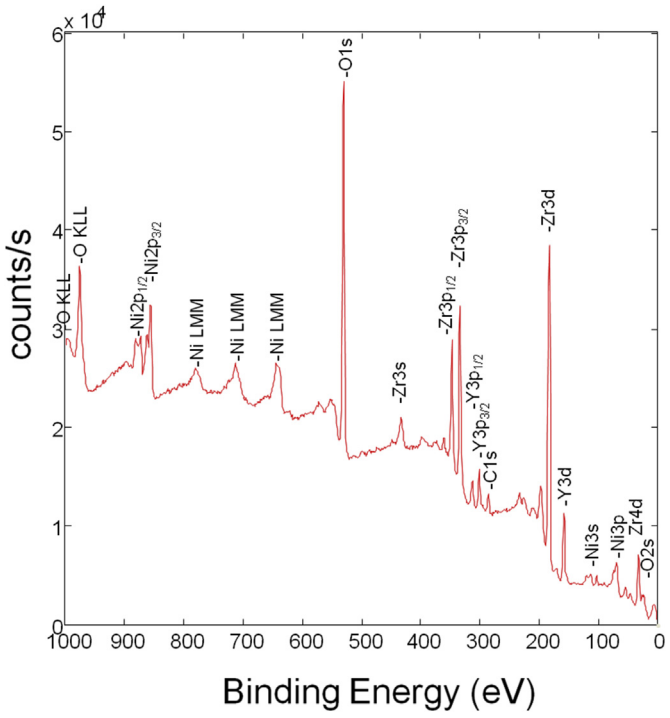

Fig. 5. XPS wide energy survey spectrum of air-side of Ni-YSZ supported sample in the as-received (oxidized) state.

advantage here for determining the amount of NiO ejected at the air/Ni-YSZ interface, as the results will be limited by line of sight to the surface. This is in contrast to energy dispersive x-ray analysis (EDX), which detects species that are as much as 1 μm below the surface.

In this study, Ni-YSZ layers, coated with a thin YSZ electrolyte layer, were first reduced from the NiO state, then oxidized fully at 900, 800, 700 or 600 °C, and then examined initially by top-down SEM analysis, as shown in Fig. 4A–D, respectively. While the NiO and YSZ phases cannot be distinguished in these 2500× magnification secondary electron images (Fig. 4), the images do indicate that the XPS analysis would be performed on relatively uniform surfaces. Thus, the morphology of the NiO-YSZ surfaces should not introduce any significant artefacts in the XPS quantification of the amount of Ni and O present on the air-side of the samples. XPS

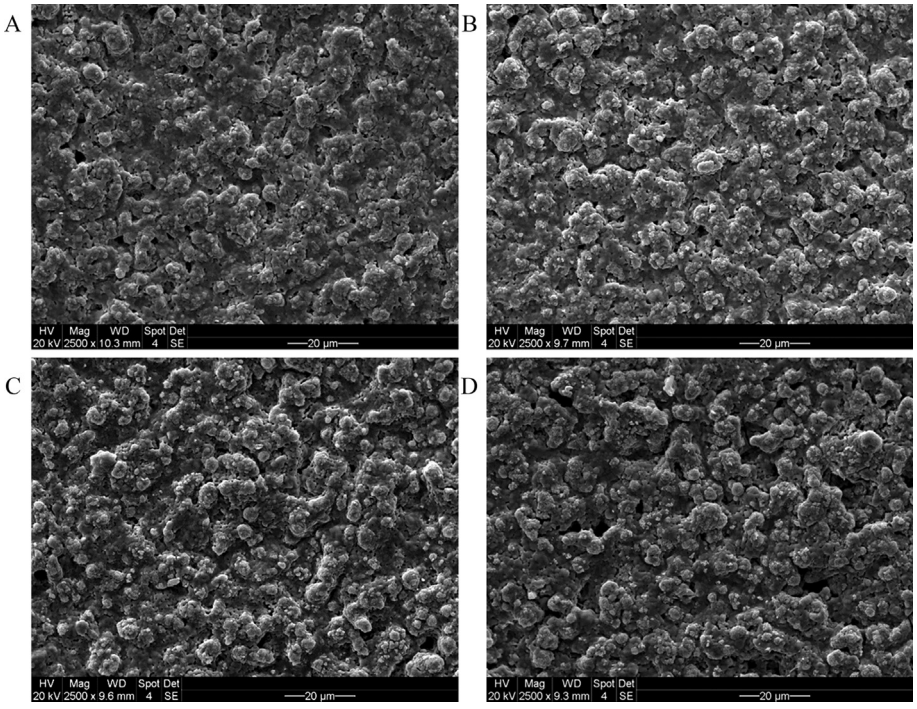

Fig. 4. SEM image of Ni-YSZ surface after full reduction in 10% H_2–He, followed by 100% Ni oxidation in 20% O_2–He at (A) 900, (B) 800, (C) 700 and (D) 600 °C.

Table 1
Summary of elemental concentrations of Ni-YSZ surface, detected using XPS.

Oxidation temp. (°C)	At% of elements detected[a]					At% without C and O[b]			Ratio of Ni:(Y + Zr)
	C	O	Ni	Y	Zr	Ni	Y	Zr	
As rec.	35.9	45.5	2.4	3.4	12.8	13	18	70	0.15
900	11.1	60.8	9.1	3.7	15.3	33	13	54	0.48
800	10.1	62.1	8.2	3.2	16.1	30	12	59	0.43
700	10.1	62.8	10.5	3.3	13.4	39	12	49	0.63
600	9.7	61.5	11.4	3.3	14.1	40	12	49	0.65

[a] From XPS peak area measurements and using the corresponding sensitivity factor.
[b] From XPS peak area measurements and the corresponding sensitivity factor, after removing the C and O signals from the calculation.

analysis should thus be able to establish whether a larger fraction of the NiO particles is ejected out of the anode/air interface onto the anode surface when oxidation occurs at low temperatures (homogeneous Ni oxidation) versus at higher temperatures (graded Ni oxidation).

An XPS wide energy survey spectrum of a typical Ni-YSZ anode support layer (ASL) surface (Fig. 4) is shown in Fig. 5 for a sample in the as-received, fully oxidized state. Peaks due to Y, Zr, O, and Ni are all seen, as expected. The presence of carbon in this spectrum is due to adventitious carbon originating from the vacuum system of the instrument. A summary of the elements detected and their relative quantities for each of the samples studied here is presented in Table 1. The first column shows the conditions used for Ni-YSZ oxidation, columns 2–6 give the relative at% of each of the elements detected, columns 7–9 provide the at% with C and O omitted, and column 10 gives the ratio of Ni to the total amount of Y and Zr present.

It is first noted in Table 1 that, in all cases, the relative amount of NiO detected at the surface after a single redox cycle is enhanced in comparison with that of the as-received sample. Second, it is clearly seen that the amount of NiO detected on the Ni-YSZ anode layer surface for the samples oxidized at 600 and 700 °C is larger than for anodes oxidized at 800 and 900 °C. This trend is seen even more clearly from the Ni:(Y + Zr) ratio (last column, Table 1), being ~0.4 for samples oxidized at 600 and 700 °C and ~0.6 for samples oxidized between 800 and 900 °C.

Fig. 6 shows the Ni 2p spectra for all four samples. The position of the Ni $2p_{3/2}$ peak at 854 ± 0.2 eV and the presence of two shake-up peaks at 856 and 861 eV on the higher binding energy side of the main Ni $2p_{3/2}$ peak is an indication of the presence of NiO in the samples [26]. The expected spectrum for metallic Ni has been added to Fig. 6, showing that metallic Ni has a peak at 852.7 eV and that its XPS signal does not have any shake-up peaks. Ni_2O_3 is likely also present in increasing concentrations as the oxidation temperature is lowered [25], with a peak that typically appears at 857 eV [27]. However, there is no evidence of this peak in Fig. 6, likely because the concentration of Ni_2O_3 in NiO that is calcined at 600 °C will be less than 0.5% [25]. The spectra for Zr and Y (not shown in Fig. 6) correspond to their oxidized states, with the peak binding energies being typical for Zr^{4+} and Y^{3+} and no major differences seen between samples.

The XPS results (Table 1) clearly show that there is a significantly higher NiO content at the air-side of the Ni-YSZ anode layer when the sample was oxidized at low temperatures (600 and 700 °C) vs. at higher temperatures (800 and 900 °C). As the low temperature oxidation conditions have been shown [22] to be correlated with a more homogeneous mechanism of oxidation of the Ni in the anode layer, with no gradient in the NiO content into the depth of the Ni-YSZ layer present at any time over the course of the oxidation process, this argues that the ejection of NiO out of the anode layer helps to prevent stresses from building up on the thin YSZ electrolyte. In the next section, the goal will be to determine whether pre-oxidation at 600 °C will force enough NiO out of a Ni-YSZ anode, containing an AFL, at the air/anode interface to decrease cracking severity in the thin YSZ electrolyte layer, which is co-sintered on the anode layer, during subsequent air exposures at 600–900 °C.

3.3. Effect of pre-oxidation cycling on subsequent air exposure damage at 600 °C

As it was demonstrated in Section 3.2 that the ejection of NiO is seen most clearly at low temperatures of oxidation (≤700 °C), it was considered that oxidizing a cell to its maximum tolerable oxidation depth prior to use in a stack may be a method of extending the life of a cell in the event that it experiences an oxidation incident in an operating cell. For clarity, the process of re-oxidizing a fully reduced Ni-YSZ anode prior to the onset of normal system operation (or possibly even before the cells are assembled into stacks) for the purpose of preventing electrolyte cracking during subsequent accidental anode air exposure is referred to here as a "pre-oxidation" cycle. The pre-oxidation step could involve multiple oxidation–reduction cycles at 600 °C in 20% O_2. In Table 2, all air exposure cycles to a safe oxidation depth (i.e., where it is known that the electrolyte will not crack), prior to an oxidation cycle to a higher oxidation depth, are still considered to be part of the pre-oxidation step.

It was previously shown [22] that, for a freshly manufactured Ni-YSZ anode-supported cell, the maximum tolerable oxidation depth of a cell, oxidized at 600 °C in 20% O_2–He without any

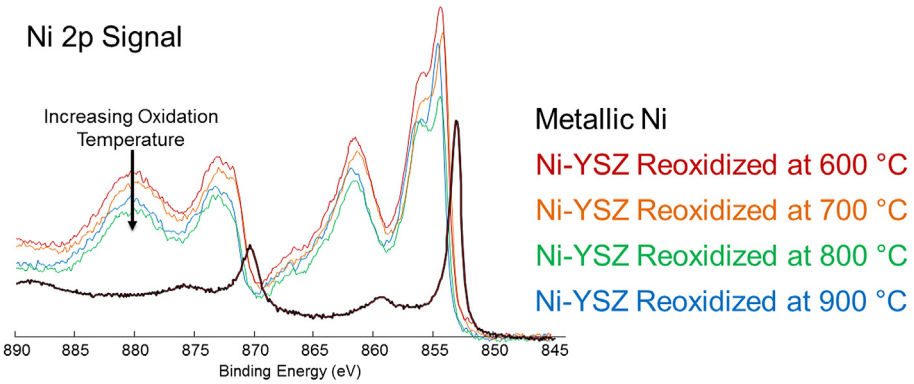

Fig. 6. XPS spectra, showing the Ni 2p peaks for as-received NiO–YSZ samples that were reduced and then re-oxidized at 600–900 °C, as well as the expected XPS spectrum for metallic Ni.

observed electrolyte cracking (in all trials), was ~74%. In the present work, this was confirmed by first fully reducing and then re-oxidizing all of the samples (15 samples, with no cathode attached) to between 74 and 78% oxidation depth at 600 °C in 20% O_2–He in a TGA (thermogravimetric analyzer). The electrolyte surface was examined using optical microscopy, as cracks in the electrolyte can typically be seen at 150× magnification. When no cracks were seen at 150× magnification, the entire electrolyte surface was carefully examined at 400× magnification to confirm that no cracks were present. It was often found that only a single crack would propagate across the electrolyte surface if an oxidation cycle went even slightly over its maximum tolerable oxidation depth. Of the ten samples oxidized to 74% (percentage of Ni in anode layer that has been oxidized), none exhibited any cracks, whereas the samples oxidized to 75 (2 samples), 76 (1 sample) and 78% (2 samples) all exhibited one or more electrolyte cracks.

Following the re-reduction of the 10 samples that exhibited no electrolyte cracking (although each sample had been exposed to one pre-oxidation cycle), a second oxidation cycle was then carried out to 80 ± 5% oxidation depth at 600 °C in air (20% O_2–He), cooled, and inspected (optical microscopy) to determine if the oxidation tolerance of the cell had changed. The results, as summarized in Table 2, indicate that the oxidation depth that could be tolerated in the second oxidation cycle (after the pre-oxidation cycle at 600 °C) did increase somewhat, from ~74% to ~80%. There was no deviation from this value from cell to cell, which were all part of the same batch. The electrolyte would consistently crack if the oxidation depth exceeded 80% in the second oxidation cycle. Thus, although the beneficial of pre-oxidation at 600 °C is seen to be minor, the oxidation tolerance of the Ni-YSZ anode layers co-sintered with an electrolyte did still increase by a small amount.

Of the ten samples that were subjected to pre-oxidation cycles to an 80 ± 5% oxidation depth at 600 °C, five cells were oxidized to ≤80% and exhibited no cracks in the electrolyte after the second oxidation step. These five samples were then subjected to a third oxidation cycle (having experienced one pre-oxidation step to 74% and an earlier pre-oxidation step to 80%) to 81 ± 2% oxidation depth. Only the two cells subjected to an 80% oxidation depth did not crack and all of the remaining cells (two oxidized to 81% and one to 83% oxidation depth) exhibited electrolyte cracking. The final two samples were subjected to seven more pre-oxidation cycles to an 80% oxidation depth, all at 600 °C in 20% O_2–He, confirmed to be crack-free, and then oxidized to 81%, after which a crack was found in the electrolyte of both samples (Table 2).

A fresh sample was then subjected to a pre-oxidation cycle that consisted of one cycle to 74% oxidation depth, followed by 20 cycles to an 80% oxidation depth, cooled, inspected to confirm that there were no cracks, and then subjected to oxidation at 81% depth. It was seen that the maximum oxidation depth that the cells could tolerate without cracking during exposure to air at 600 °C remained at 80%. Multiple pre-oxidation cycles did not appear to have any beneficial effects on the tolerable oxidation depth of the Ni-YSZ ASL, even after as many as 20 pre-oxidation cycles.

A 50% O_2–He atmosphere was then examined as an alternative condition for the pre-oxidation step, since it was suggested in our prior study [22] that the degree of homogeneity of the Ni oxidation into the anode layer would then be higher. As it is hypothesized that increasing the homogeneity of the Ni oxidation will increase the amount of NiO ejected at the air/Ni-YSZ interface, this should also have increased the oxidation tolerance of the cell. However, it is seen in Table 2 that the exposure of the samples to this high pO_2 environment did not have any effect on the tolerable oxidation depth, which remained at ~80%. In consideration of the anode surface NiO content, determined by XPS analysis (Fig. 6, Table 1), this is not surprising, since there was no increase observed when the temperature was decreased from 700 to 600 °C.

It can therefore be concluded that there is a small benefit to the exposure of a Ni-YSZ anode-supported cell to a single pre-oxidation treatment step at 600 °C in terms of increasing the subsequent oxidation depth that the cell can tolerate. For the cells used in this study, the oxidation tolerance was increased from 74 to 80% before the YSZ electrolyte was seen to crack. There are, however, no obvious benefits to the use of multiple pre-oxidation steps and, further, the use of a higher pO_2 for the pre-oxidation cycle also provides no further protection to the cell in subsequent oxidation cycles. This suggests that the majority of the NiO that is ejected out of the anode-air interface does so in the first oxidation cycle.

The source of this ~5% increase in oxidation tolerance is proposed to be due to small changes in the Ni content in the surface region of the anode, which, if left within the pore structure of the anode, would have increased the overall internal stress in the anode layer. It has been demonstrated here that increasing the number of pre-oxidation cycles does not improve the oxidation tolerance of the cell at 600 °C after the first cycle. Thus, it is likely that it is not possible to eject more NiO out of the anode surface, as the NiO particles would then have to be extracted from the inner regions of the anode layer.

3.4. Effect of pre-oxidation cycles on subsequent air exposure damage at 800 °C

When Ni-YSZ anode-supported cells are oxidized under conditions that result in a graded NiO content into the anode over the course of exposure to air at high temperatures or low pO_2, it was shown previously [22] that the oxidation tolerance is then very low. Under these conditions, cracks that run parallel to the edge of the

Table 2
Summary of maximum oxidation depth that the YSZ electrolyte can tolerate without cracking after various "homogeneous" Ni-YSZ anode pre-oxidation treatments, all at 600 °C.

Sample	Number of samples tested	Pre-oxidation depth			Final oxidation depth[a]	Oxidation tolerance[b]
		Cycle 1	Cycle 2	Cycles 3–10		
"Fresh" cell (no pre-oxidation)	15	–	–	–	74–78%	74%
1 Pre-oxidation cycle[c]	15	74	–	–	80 ± 5%	80%
2 Pre-oxidation cycles[c]	10	74	80	–	81 ± 1%	80%
10 Pre-oxidation cycles[c]	5	74	80	80	81 ± 0.5%	80%
20 Pre-oxidation cycles[c]	1	74	80	80	81%	80%
50% pO_2 Pre-oxidation cycles[c]	2	74	80	80	81%	80%

[a] Range of oxidation depths (percentage of total Ni in anode layer that has been oxidized) to which the samples were subjected.
[b] Allowable sample oxidation depth before YSZ cracking was observed.
[c] Pre-oxidation cycles involved one or more Ni partial oxidation steps of a Ni-YSZ anode at 600 °C, and this was followed by oxidation to the 'Final Oxidation Depth' to determine if the oxidation tolerance changes.

cell develop when <50% of the Ni in the anode is oxidized and propagate across the electrolyte surface when only 60% of the Ni is oxidized [22]. These first cracks form because air can penetrate from the sides of the sectioned fragments where the local oxidation depth is likely >74%, even though the overall anode oxidation depth is <50%.

It has been demonstrated above that the oxidation tolerance of a fresh sample, oxidized under conditions in which Ni is oxidized more homogeneously in the anode layer (Table 1), can be improved from ~74% to ~80% after a single pre-oxidation cycle at 600 °C, likely because of NiO particle ejection out of the anode-air interface during the oxidation process. Since NiO particle ejection occurs at all anode-air interfaces, including at the sample edges, a pre-oxidation cycle should, in theory, have a large effect on the formation of these edge cracks. This is because the internal stresses in the anode in this region should then have been significantly lowered. Thus, the oxidation tolerance of a cell should be dramatically improved when exposed to oxidation conditions that lead to a NiO gradient during air exposure of the anode layer.

In this part of the work, the effect of a pre-oxidation cycle at 600 °C on the subsequent electrolyte cracking characteristics observed during air exposure at 800 °C was investigated. Two fresh samples were prepared and then oxidized using two different procedures. Fig. 7 shows the electrolyte surface of the first sample after it was subjected to one full oxidation cycle at 800 °C. It can be seen that the electrolyte cracks, in Fig. 7A, are primarily parallel to the edge of the sample (left side). Many cracks are also seen that are perpendicular to the edge of the sample, with these cracks shown previously [22] to propagate from one parallel crack to another. However, since these cracks do not propagate linearly through the parallel cracks, it is evident that the parallel cracks formed first. In the central regions of the sample (Fig. 7B), it can be seen that the electrolyte surface has many wide cracks that have randomly propagated across the electrolyte surface, evidence of the severity of the degradation under these conditions.

Fig. 8 shows the electrolyte of the second fresh sample, which was subjected to a single pre-oxidation cycle at 600 °C (74% of the total Ni content has been oxidized), followed by full oxidation of the Ni in the anode at 800 °C. It can be seen in Fig. 8A that there are still cracks running parallel to the sample edge (left side), except that there are only two, in comparison with five cracks for the sample oxidized at 800 °C but without a pre-oxidation cycle (Fig. 7A). In Fig. 8B, it can be seen that the cracks that have randomly propagated through the central regions of the electrolyte are narrower than those in the sample that was not pre-oxidized (Fig. 7B) and there also appears to be fewer cracks produced overall.

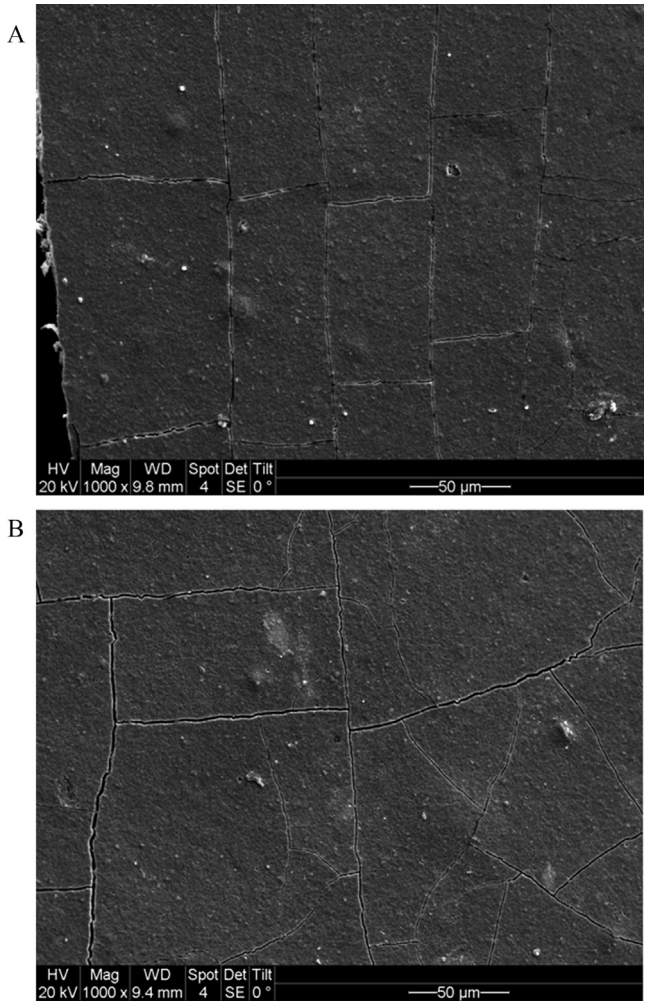

Fig. 7. Cracks seen on the electrolyte surface (top down view of the sample) of a sample that was subjected to a full oxidation cycle (100% NiO) at 800 °C, with SEM images shown at (A) the edge of sample and (B) in the central area of the electrolyte surface.

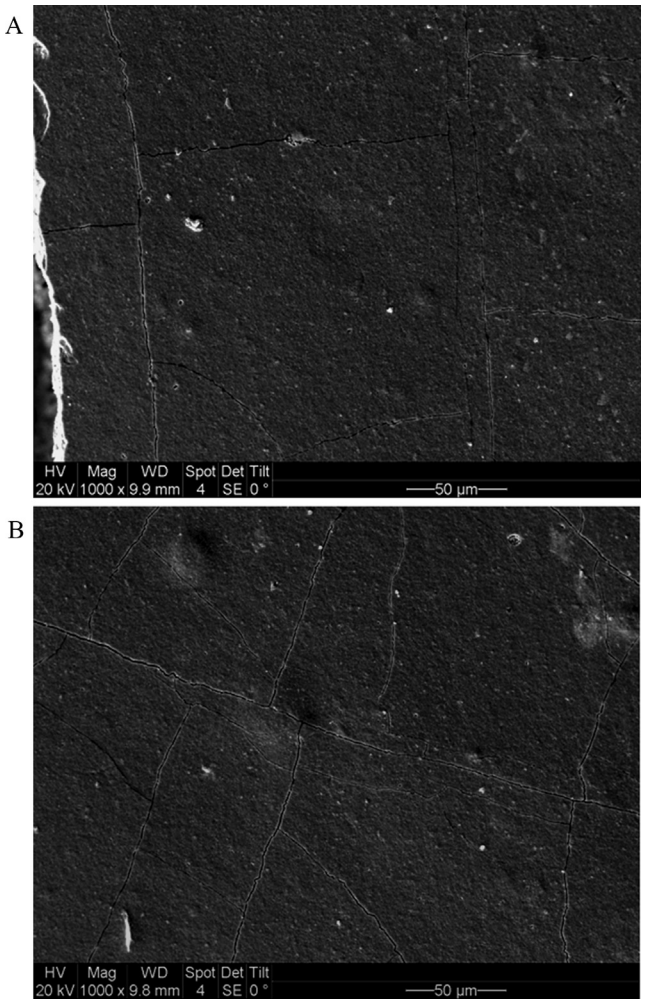

Fig. 8. Cracks seen on the electrolyte surface (top down view of the sample) of a sample that was subjected to one pre-oxidation cycle to an oxidation depth of 74% at 600 °C, followed by a full oxidation cycle at 800 °C, with SEM images shown at (A) the edge of sample and (B) in the central area of the electrolyte surface.

In fact, in the central regions of the electrolyte, the total number of cracks (of any length) visible in the SEM image has decreased, from 22 to 13, for a sample that had not been pre-oxidized (Fig. 7B) versus one that had (Fig. 8B). This decrease in the number of cracks in the viewable area of the micrograph and the narrower crack widths (Fig. 8B vs. Fig. 7B) demonstrate that there is a decrease in the severity of electrolyte degradation when samples were pre-oxidized at 600 °C and then oxidized fully at 800 °C.

While the irregular shape of the samples used in this study did not affect the observed cracking, gas permeation testing was not possible. However, further evidence that the cracks are more numerous and wider when a pre-oxidation cycle was not applied (Fig. 7) versus after such a cycle (Fig. 8) is seen in Fig. 9. Here, the rate of reduction after the oxidation cycle at 800 °C (a), determined by TGA, is faster than for the sample that was pre-oxidized and then subjected to an oxidation cycle at 800 °C (b). This higher reduction rate (Fig. 9(a)) is evidence of enhanced penetration of H_2 through the wider and more numerous cracks in the electrolyte after the oxidation cycle at 800 °C with no pre-oxidation step employed.

However, while the oxidation tolerance at 800 °C may have been slightly improved after a pre-oxidation cycle at 600 °C, any amount of cracking of the electrolyte can be very harmful to the life and performance of an anode-supported SOFC. Thus, it is necessary to determine if the pre-oxidation step has improved the oxidation tolerance of a Ni-YSZ anode-supported cell. Once again, fresh samples were prepared and subjected to a pre-oxidation step at 600 °C, followed by partial oxidation (40–60%) at 800 °C in air. Not surprisingly and similar to the case in Fig. 8A, the severity of degradation is lower, as only two parallel cracks are seen (versus the five that are normally observed). However, in each case, cracks parallel to the edge of the sample formed at only a 40% oxidation depth, indicating that the oxidation tolerance had not been improved.

To attempt to further enhance NiO ejection out of the anode-air interface, 20 pre-oxidation cycles were applied, using a 74% depth of oxidation in the first cycle and 80% in the remaining 19 cycles, all at 600 °C and in 50% O_2–He. These cells were cooled and inspected with optical microscopy to ensure that they were crack-free, and then re-heated to 800 °C. Although it was demonstrated in the previous section that a similar multi-step pre-oxidation procedure was unsuccessful in improving the oxidation tolerance at 600 °C, it was theorized that, since the first cracks to form are at the edges of the sample (Fig. 8A), this procedure could have more success for samples oxidized subsequently at 800 °C.

Fig. 10A shows that, for a sample that was oxidized to a 50% oxidation depth at 800 °C after 20 pre-oxidation cycles at 600 °C, there are only two cracks that propagate parallel to the sample edge at the bottom of the image, as compared to five cracks in the electrolyte of the fresh sample that had been oxidized to 50% without pre-oxidation (Fig. 10B). This decrease in the number of cracks is consistent with what was seen after a single pre-oxidation step at 600 °C to a 74% oxidation depth in Fig. 8A and B.

Overall, contrary to the enhanced oxidation tolerance observed at 600 °C after the application of one or more pre-oxidation cycles, also at 600 °C (Section 3.3), there appear to be no significant benefits (in terms of stopping electrolyte cracking) obtained from the pre-oxidation treatment when the Ni-YSZ anode layer underwent air exposure at 800 °C. This somewhat negative outcome may be related to the rather narrow definition of 'oxidation tolerance', used in this work, i.e., the highest oxidation depth that can be tolerated at a particular temperature before any cracks begin to appear. In fact, it is noted that the severity of the electrolyte cracking during Ni-YSZ oxidation at 800 °C was almost halved after the use of a pre-oxidation step. This, in turn, may be enough to significantly extend the life of an operating fuel cell, as long as the extent of leakage of fuel or air through the cracks remains relatively minor.

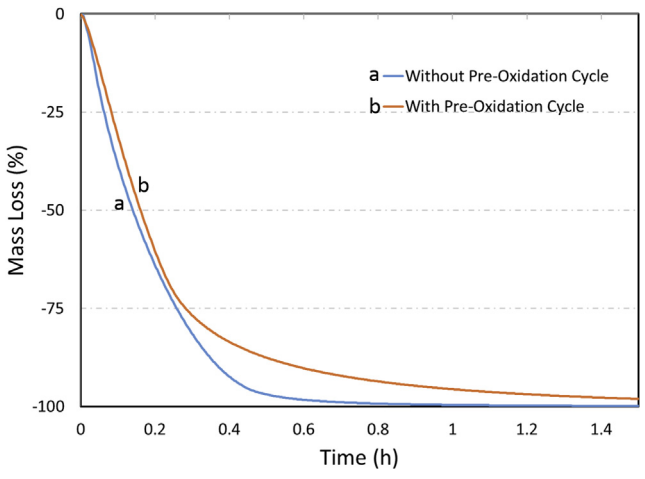

Fig. 9. Thermogravimetric analysis data showing mass loss with time during NiO reduction in H_2 at 800 °C. The sample that has (a) not been exposed to a pre-oxidation cycle exhibits a more rapid rate of reduction than the sample that has (b) had been exposed to a pre-oxidation cycle at 600 °C prior to being oxidized at 800 °C.

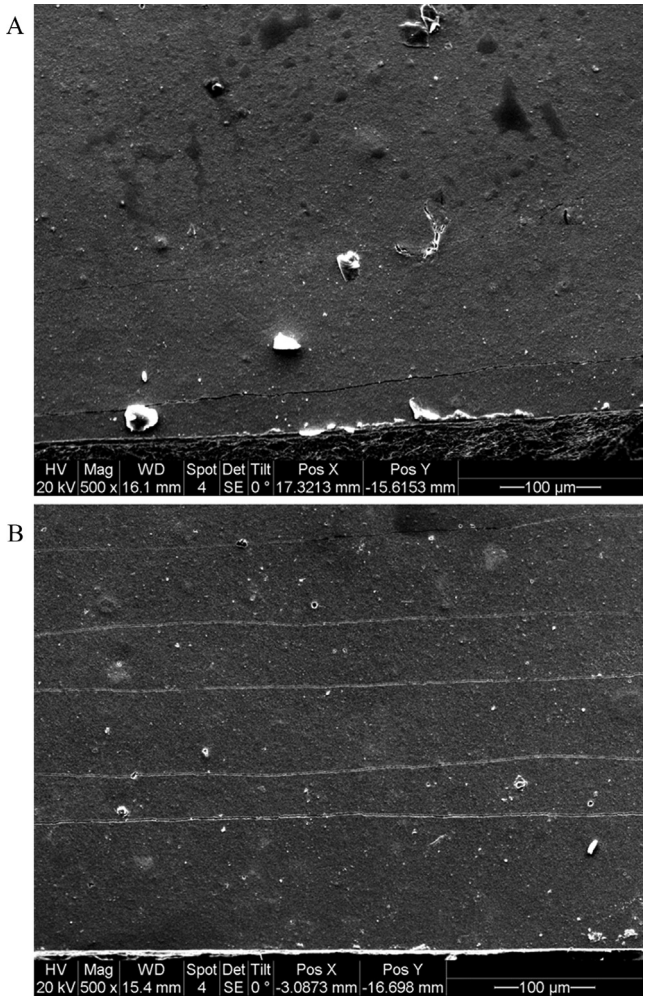

Fig. 10. Cracks seen in the YSZ electrolyte of a Ni-YSZ ASL/YSZ sample that was air-exposed to a 50% oxidation depth at 800 °C in 20% O_2–He, comparing images after (A) 20 pre-oxidation cycles at 600 °C in 50% O_2–He and (B) without a pre-oxidation treatment.

4. Conclusions

When a Ni-YSZ (yttria-stabilized zirconia) anode-supported solid oxide fuel cell (SOFC) is inadvertently exposed to air, the outcome can be the catastrophic degradation of the cells, resulting from the 70% volume expansion of Ni as it forms NiO. The most critical degradation mechanism in high porosity Ni-YSZ anodes has been found to be cracking of the thin YSZ electrolyte layer. It had previously been observed that the more homogeneously distributed the NiO is within the anode layer over the course of air exposure, the lower the degree of cell degradation observed (fewer and narrower cracks in the YSZ electrolyte).

The reason that the homogeneously oxidized anode produces fewer cracks was theorized to result from the ejection of NiO particles out to the surface of the anode during air exposure, thus relieving some of the internal stresses. X-ray photoelectron spectroscopy analysis was used here to determine the NiO content on the outer surface of a Ni-YSZ anode-support layer, specifically monitoring the ratio of NiO content relative to Y and Zr (Ni:(Y + Zr)). It was confirmed that the Ni:(Y + Zr) ratio at the anode-air interface increases when the Ni-YSZ anode is exposed to oxidizing conditions that lead to a homogeneous Ni/NiO distribution throughout the anode for the entire duration of the oxidation cycle.

It is also shown here that samples that were pre-oxidized in a single step at 600 °C to a ~74% oxidation depth were crack-free and undamaged after subsequent air exposure at 600 °C, at least up to an oxidation depth (percentage of total Ni in the anode layer that has been oxidized) of 80%. This increase of ~6% in the oxidation tolerance of the Ni-YSZ anode layer does not seem to be a significant improvement, but it could still represent the difference between saving or damaging a cell in some situations.

When pre-oxidation was carried out at 600 °C prior to anode oxidation at a higher temperature, e.g., 800 °C, cracks still appeared when <50% of the Ni in the anode had been oxidized, similar to what was seen without a re-oxidation step. However, the cracks that were seen in the electrolyte following a full anode oxidation step at 800 °C (following the pre-oxidation step) were less severe (narrower and fewer in number) than when no pre-oxidation treatment was used. This could equate to a significant improvement in lifespan of a cell, as long any fuel or air leakage that occurs through the electrolyte cracks does not reach a critical magnitude (i.e., if the output power of the cell is not significantly decreased).

Acknowledgments

We gratefully acknowledge the Natural Sciences and Engineering Research Council of Canada (NSERC) for the support of this work through funding to the NSERC SOFC Canada Strategic Research Network. This work was also supported by an equipment and infrastructure grant from the Canadian Foundation for Innovation (CFI) and the Alberta Science and Research Authority. We also thank V. Vedasri and Dr. S. Paulson (University of Calgary) for valuable discussions, and Drs. M. Schoel and T. Furstenhaupt (both at the University of Calgary) for assistance with the SEM analyses.

References

[1] A. Atkinson, S. Barnett, R.J. Gorte, J.T.S. Irvine, A.J. McEvoy, M. Mogensen, S.C. Singhal, J. Vohs, Nat. Mater. 3 (2004) 17–27.
[2] M. Cassidy, K. Kendall, G. Lindsay, First European Solid Oxide Fuel Cell Forum: a Platform for Science, Engineering and Technology, 3–7 October 1994, pp. 577–586. Lucerne, Switzerland.
[3] N.Q. Minh, R.A. Gibson, First European Solid Oxide Fuel Cell Forum: a Platform for Science, Engineering and Technology, 3–7 October 1994, pp. 587–596. Lucerne, Switzerland.
[4] D. Fouquet, A.C. Muller, A. Webber, E. Ivers-Tiffée, Ionics 8 (2003) 103–108.
[5] D. Waldbillig, A. Wood, D.G. Ivey, Solid State Ionics 176 (2005) 847–859.
[6] J.L. Young, V. Vedaharathinam, S. Kung, S. Xia, V.I. Birss, ECS Trans. 7 (2007) 1511–1519.
[7] M. Pihlatie, A. Kaiser, M. Mogensen, Solid State Ionics 222–223 (2012) 38–46.
[8] T. Klemenso, C.C. Appel, M. Mogensen, J. Electrochem. Soc. 152 (2005) A2182–A2192.
[9] K. Haltiner, S. Mukerjee, D. England, M. Faville, S. Kelly, B. Edlinger, J. Tachtler, U.S. Patent 6,744,235 filed Jun 24, 2002, and issued Jun 1, 2004.
[10] A. Wood, M. Pastula, D. Waldbillig, D.G. Ivey, J. Electrochem. Soc. 153 (2006) A1929–A1934.
[11] D. Waldbillig, A. Wood, D.G. Ivey, J. Electrochem. Soc. 154 (2007) B133–B138.
[12] N. Tikekar, T. Armstrong, A. Virkar, J. Electrochem. Soc. 153 (2006) A654–A663.
[13] D. Sarataradis, A. Atkinson, Fuel Cells 7 (2007) 246–258.
[14] M. Pihlatie, T. Ramos, A. Kaiser, J. Power Sources 193 (2009) 322–330.
[15] M. Ettler, G. Blass, N.H. Menzler, Fuel Cells 7 (2007) 349–355.
[16] D. Sarataradis, R.J. Chater, A. Atkinson, J. Electrochem. Soc. 155 (2008) B467–B472.
[17] M. Pihlatie, A. Kaiser, P.H. Larson, M. Mogensen, J. Electrochem. Soc. 156 (2009) B322–B329.
[18] T. Klemenso, C. Chung, P.H. Larson, M. Mogensen, J. Electrochem. Soc. 152 (2005) A2186–A2192.
[19] A. Faes, A. Nakajo, A. Hessler-Wyser, D. Dubois, A. Brisse, S. Modena, J. Van Herle, J. Power Sources 193 (2009) 55–64.
[20] J. Laurencin, G. Delette, B. Morel, F. Lefebvre-Joud, M. Dupeux, J. Power Sources 192 (2009) 344–352.
[21] D. Sarataradis, R.A. Rudkin, A. Atkinson, J. Power Sources 180 (2008) 704–710.
[22] J.L. Young, V.I. Birss, J. Power Sources 196 (2011) 7126–7135.
[23] D. Simwonis, H. Thülen, F.J. Dias, A. Naoumidis, D. Stöver, J. Mater. Process. Technol. 92–93 (1999) 107–111.
[24] J.A. Rodriguez, J.C. Hanson, A.I. Frenkel, J.Y. Kim, M. Perez, J. Am. Ceram. Soc. 124 (2002) 346.
[25] A. Illis, G.C. Nowlan, H.J. Koehler, Can. Inst. Min. Met. Bull. 73 (1970) 49–53.
[26] J.C. Klein, D.M. Hercules, J. Catal. 82 (1983) 424–441.
[27] D.H. Lee, S.Y. Yoon, D.H. Yoon, S.J. Suh, J. Korean Phys. Soc. 44 (2004) 1079–1082.